ChemComm

Chemical Communications

www.rsc.org/chemcomm

Volume 49 | Number 100 | 28 December 2013 | Pages 11709–11830

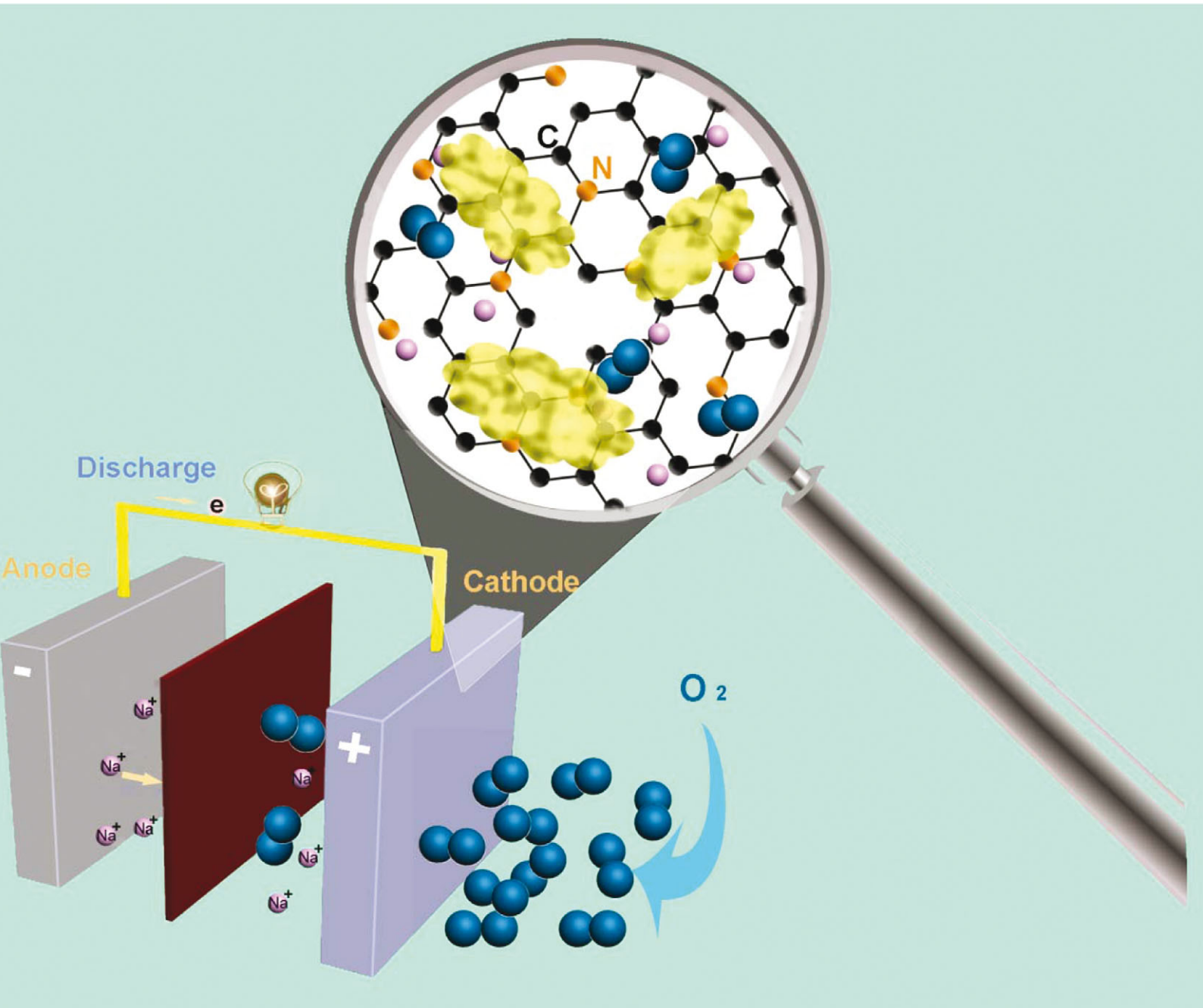

ISSN 1359-7345

RSC Publishing

COMMUNICATION

Xueliang Sun *et al.*

Superior catalytic activity of nitrogen-doped graphene cathodes for high energy capacity sodium–air batteries

ChemComm

RSC Publishing

COMMUNICATION

View Article Online
View Journal | View Issue

Cite this: *Chem. Commun.*, 2013, **49**, 11731

Received 29th August 2013,
Accepted 3rd October 2013

DOI: 10.1039/c3cc46606j

www.rsc.org/chemcomm

Superior catalytic activity of nitrogen-doped graphene cathodes for high energy capacity sodium–air batteries†

Yongliang Li, Hossein Yadegari, Xifei Li, Mohammad N. Banis, Ruying Li and Xueliang Sun*

Nitrogen-doped graphene nanosheets (N-GNSs) displayed a discharge capacity two times greater than their pristine counterpart, as well as superior electrocatalytic activity as a cathode material for sodium–air batteries. The enhanced performance of N-GNSs is attributed to the active sites introduced by nitrogen doping.

Nonaqueous lithium–air batteries have been intensively studied for the past few years due to their extremely high energy density, making them suitable candidates for electric vehicles (EVs) and hybrid electric vehicles (HEVs).[1] However, the discharge products are insoluble in the electrolyte but deposit on the electrode, resulting in blocked oxygen diffusion channels and subsequent reaction termination.[2] One of the challenges in improving the battery performance is the development of optimum cathode materials with ideal morphology, conductivity, surface area, porosity, *etc.* However, large overpotentials are observed during the discharge and charge processes, leading to relatively low round-trip energy storage efficiencies. In addition, the limited amount of lithium resource available inevitably prevents lithium–air batteries from wide applications in EVs and HEVs.[3] Recently, studies on replacing lithium with sodium for an alternative metal–air battery has been reported with promising results. Sodium is an earth abundant material with modest cost, and sodium–air batteries have been shown to deliver an energy density of about 1600 W h kg^{-1}, holding the same great promise as lithium–air batteries meeting the rapidly growing energy demand required for future automotive applications.[4] Similar to lithium–air batteries, the discharge product in sodium–air batteries will also result in product deposition on the electrode surface, therefore, the properties of the cathode material are crucial in determining the battery performance. For example, Fu *et al.* demonstrated that graphene nanosheets (GNSs) used as a cathode material in sodium–air batteries cause an increase in discharge capacity compared to a normal carbon film electrode due to the unique chemical and physical properties of GNSs.[5]

In our previous study, we showed that chemical doping using nitrogen atoms to carbon materials results in a modification to the electronic property of the material while also providing a greater number of active sites, resulting in enhanced interaction between the carbon structure and other molecules, ultimately leading to improved performance in lithium–air batteries.[6] It is expected that nitrogen doping into a carbon cathode can also increase the performance in sodium–air batteries. However, to the best of our knowledge, there are few reports about the heteroatom-doping effect of carbon materials for sodium–air batteries. Herein, nitrogen-doped graphene nanosheets (N-GNSs) were employed as cathode materials for sodium–air batteries. We found that N-GNSs demonstrated excellent electrocatalytic activity for the oxygen reduction reaction (ORR), delivering a discharge capacity two times greater than that for GNSs. This finding indicates that N-GNSs are promising electrode materials. Furthermore, this study also implies that modification to carbon materials is a rational approach towards improving the performance of sodium–air batteries.

Fig. 1a shows the discharge curves of GNS and N-GNS electrodes in sodium–air cells at current densities of 75, 150, and 300 mA g^{-1}, respectively. N-GNS electrodes consistently deliver higher discharge capacities for all current densities; for example, the discharge capacity at 75 mA g^{-1} was about 8600 mA h g^{-1}, which is about two times greater than that for the GNS electrode (4350 mA h g^{-1}). With increasing current density, the discharge capacity decreases for both electrode materials. The discharge capacity of the N-GNS electrode decreases to 6000 mA h g^{-1} at 150 mA g^{-1}, and 3980 mA h g^{-1} at 300 mA g^{-1}. However, they are still higher than those of GNSs, which are 2550 and 990 mA h g^{-1} at 150 and 300 mA g^{-1}, respectively. The average discharge voltages of N-GNS electrodes are also higher than those of GNS electrodes at different current densities. Recent studies have indicated that oxygen adsorption is the first step before the initial charge transfer process for carbonaceous materials, and ORR preferentially takes place at defective sites.[7] As shown in Fig. S1 (ESI†), the intensity ratio of D to G bands of GNSs and N-GNSs are 0.96 and 1.10, respectively, confirming that more defects are

Department of Mechanical and Materials Engineering, The University of Western Ontario, ON, N6A 5B9, Canada. E-mail: xsun@eng.uwo.ca; Fax: +1-519-661-3020; Tel: +1-519-661-2111 ext. 87759

† Electronic supplementary information (ESI) available: Experimental details and data on the physical properties. See DOI: 10.1039/c3cc46606j

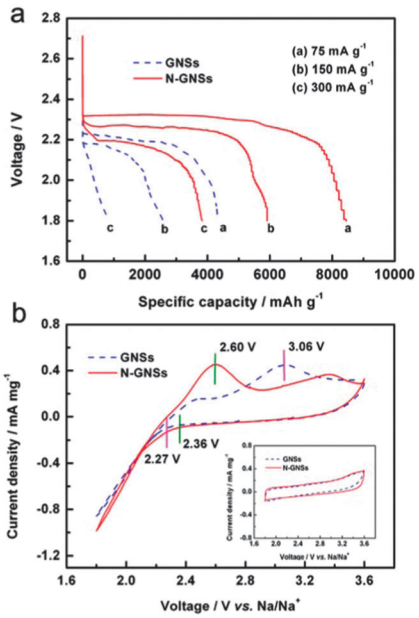

Fig. 1 (a) The voltage profiles and (b) CV curves of GNS and N-GNS electrodes.

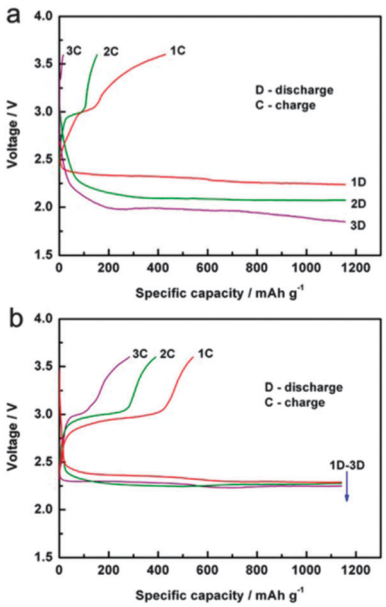

Fig. 2 Charge–discharge performance of initial three cycles of (a) GNS and (b) N-GNS electrodes at 75 mA g^{-1}.

obtained after nitrogen doping, resulting in the increase in discharge voltages. The CV curves of GNS and N-GNS electrodes in an argon or oxygen atmosphere are shown in Fig. 1b. There are no obvious cathodic and anodic peaks in the CVs of both samples tested in argon; however, reduction reactions occur after introducing oxygen into the system. The onset potential of ORR for GNSs is ~2.27 V while for N-GNSs, the onset potential of ORR positively shifts to ~2.36 V, indicating superior electrocatalytic activity of N-GNSs towards ORR.[8] It is important to note that the anodic peak, corresponding to the oxidation of the discharge product, for the N-GNS electrode is at ~2.60 V, a value which is ~0.46 V negatively shifted in comparison to the GNS electrode. This indicates that N-GNSs show better electrocatalytic activity towards the oxygen evolution reaction (OER) as well.

The cyclability of sodium–air batteries utilizing GNS and N-GNS electrodes was studied by cycling at a low depth of discharge with a cut-off of 1150 mA h g^{-1} (Fig. 2). It is clearly shown that the discharge plateaus during the first three cycles for the N-GNS electrode is decreased only slightly while a much more pronounced decline is observed for the GNS electrode. During the charge process, the N-GNS electrode demonstrates lower charge voltages and higher charge capacity compared to the GNS electrode. These results indicate that N-GNSs display higher bifunctional electrocatalytic activities for both ORR and OER than GNSs.

In order to study the electrochemical polarization of GNS and N-GNS electrodes, electrochemical impedance spectroscopic (EIS) analysis was conducted. The Nyquist plots for cells employing two samples as electrode materials obtained after the first discharge are shown in Fig. S2 (ESI†). Both plots exhibit two semicircles followed by a linear part, which is caused by the dispersion of three different processes with different time constants.[9] The EIS spectra are fitted using an equivalent circuit (inset of Fig. S2, ESI†) and the obtained parameters are listed in Table S1 (ESI†). Comparison of fitted parameters indicates that the electrolyte resistance is similar for GNS and N-GNS electrodes; however, there are significant differences for other circuit parameters. The interface resistance of the N-GNS electrode is higher than that of the GNS electrode, indicating the formation of more discharge products on the former electrode, which is consistent with the results for discharge capacities. The N-GNS electrode has a lower value of charge-transfer resistance, R_{ct}, which is related to the conductivity of the discharge products, regardless of more discharge products. The reason behind this finding will be discussed in the following section. However, from the impedance results, it is suggested that the GNS electrode should have larger electrochemical polarization than the N-GNS electrode due to higher charge-transfer resistance.

Fig. 3a and b show the morphology of the discharge products on GNS and N-GNS electrodes, respectively. The particle size of discharge products on GNSs is 200–300 nm while it is ~50 nm on N-GNSs. In our previous study on N-GNSs as electrode materials for lithium–air batteries, we found similar results that the particle size decreased after doping nitrogen into GNSs and the reason is that the discharge products most likely prefer to nucleate and grow around the defective sites.[10] As seen from Fig. 3c and d after 12 h discharge, discharge products dispersed more uniformly on the N-GNS surface with smaller particle size of 5–10 nm while aggregation of particles were observed on GNSs (indicated by blue circles). XRD patterns of GNS and N-GNS electrodes before and after discharge are shown in Fig. 3e. The additional peaks for both electrodes after discharge are assigned to Na_2O_2, and the results are consistent with the report by other groups.[5] It was reported that the nature and morphology of the discharge product of lithium–air batteries significantly affects the charge overpotential, *i.e.* the lithium deficient Li_2O_2 surface shows a low charge overpotential while better interaction between discharge products and carbon surface also decreases the charge overpotential.[11] There is no information on the electrical transport properties of Na_2O_2 due to sodium vacancy or deficiency and further study is required.

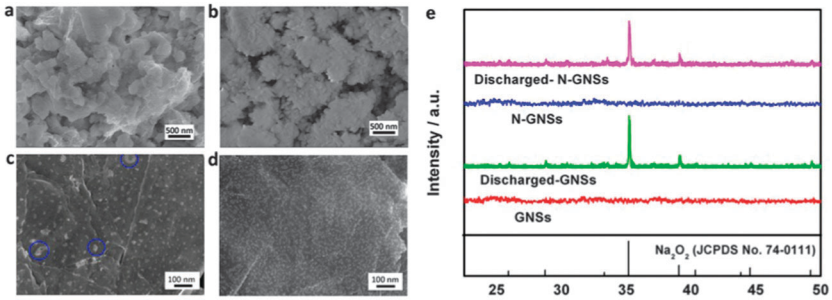

Fig. 3 SEM images of the fully discharged (a) GNSs, (b) N-GNS electrodes and (c) GNSs, (d) N-GNS electrodes discharged for 12 h; (e) XRD patterns of pristine and discharged GNS and N-GNS electrodes.

However, it is believed that the difference in morphology on GNS and N-GNS electrodes, as well as the enhanced contact for discharge products on the N-GNS surface due to the increased number of defective sites, should result in a lower overpotential/polarization.

The morphology of discharge products at various current densities were observed by SEM (Fig. S3, ESI†). In addition to particles with a size of ~50 nm in diameter on the carbon surface, larger particles (100–300 nm) also appear on top of the smaller particles at 150 mA g^{-1}. However, an increase in current density to 300 mA g^{-1} resulted in the formation of a film rather than individual particles. The reaction pathway leading to Na_2O_2 could be described as:[12]

$$2Na^+ + 2e^- + O_2* \rightarrow Na_2O_2* \quad (1)$$

where * refers to a surface adsorbed species. Firstly, Na_2O_2* forms on the surface of carbon. If the solubility of Na_2O_2* in the electrolyte is zero, the resulting products will permanently remain on the reaction sites. As the discharge continues, the number of active sites available for Na_2O_2 deposition will continually decrease, and eventually lead to a continuous increase in overpotential during discharge.[13] Therefore, the discharge products would re-dissolve into the electrolyte *via* solvation.[11] The formation of aggregated particles during discharge also gives evidence towards this idea, and also indicates that growth of the discharge product on carbon surfaces does not follow a simple mechanism.

The growth mechanism and the different morphology of discharge products is proposed and shown in Fig. S4 (ESI†). At low current density, the charge-transfer rate from the surface is slow, resulting in a slow formation rate for Na_2O_2. When the concentration of the solvated Na_2O_2 exceeds the solubility limit, precipitation onto carbon materials occurs (Fig. S3C, ESI†). At high current density, a large amount of Na_2O_2 is generated on the surface, and may undergo surface migration, resulting in the formation of a very uniform film (Fig. S3D, ESI†). For current densities between the two extremes, competition between solvation, precipitation and migration takes place. A similar mechanism for the morphological differences of discharge products in lithium–air batteries has been proposed by Nazar *et al.*, however, it is believed that the exact growth of Na_2O_2 is more complicated and further study is needed.[11]

In summary, we reported the superior performance of N-GNSs as cathode materials for sodium–air batteries in comparison to GNSs. It was demonstrated that the improvement was due to the defective sites introduced by nitrogen doping. The morphology of the discharge products on N-GNS electrodes is different from that on GNS electrodes, and the discharge product distribution is more uniform accompanied with smaller particle size. The formation of the discharge products on N-GNSs at different current densities resulted from various processes, including solvation, precipitation and migration. We believe that heteroatom-doping to carbon cathodes is a rational direction to modify other substrate materials for sodium–air batteries.

This research was supported by Natural Sciences and Engineering Research Council of Canada, Canada Research Chair Program, Canada Foundation for Innovation and the University of Western Ontario. The authors are indebted to Andrew Lushington for the discussion.

Notes and references

1 K. Abraham and Z. Jiang, *J. Electrochem. Soc.*, 1996, **143**, 1; Y. Li, J. Wang, X. Li, D. Geng, R. Li and X. Sun, *Chem. Commun.*, 2011, **47**, 9438.
2 R. Williford and J. Zhang, *J. Power Sources*, 2009, **194**, 1164; R. Mitchell, B. Gallant, C. Thompson and Y. Shao-Horn, *Energy Environ. Sci.*, 2011, **8**, 2952.
3 P. Hartmann, C. Bender, M. Vračar, A. Dürr, A. Garsuch, J. Janek and P. Adelhelm, *Nat. Mater.*, 2013, **12**, 228.
4 J. Kim, H. Lim, H. Gwon and K. Kang, *Phys. Chem. Chem. Phys.*, 2013, **15**, 3623; Q. Sun, Y. Yang and Z. Fu, *Electrochem. Commun.*, 2012, **16**, 22.
5 W. Liu, Q. Sun, Y. Yang, J. Xie and Z. Fu, *Chem. Commun.*, 2013, **49**, 1951.
6 Y. Li, J. Wang, X. Li, D. Geng, J. Yang, R. Li and X. Sun, *Electrochem. Commun.*, 2011, **13**, 668; Y. Li, J. Wang, X. Li, D. Geng, M. Banis, R. Li and X. Sun, *Electrochem. Commun.*, 2012, **18**, 12.
7 S. Nakanishi, F. Mizuno, T. Abe and H. Iba, *Electrochemistry*, 2012, **80**, 783; Y. Lu, B. Gallant, D. Kwabi, J. Harding, R. Mitchell, M. Whittingham and Y. Shao-Horn, *Energy Environ. Sci.*, 2013, **6**, 750.
8 C. Rao, C. R. Cabrera and Y. Ishikawa, *J. Phys. Chem. Lett.*, 2010, **1**, 2622.
9 N. Takami, A. Satoh, M. Hara and T. Ohsaki, *J. Electrochem. Soc.*, 1995, **142**, 371.
10 J. Xiao, D. Mei, X. Li, W. Xu, D. Wang, G. Graff, W. Bennett, Z. Nie, L. Saraf, I. Aksay, J. Liu and J. Zhang, *Nano Lett.*, 2011, **11**, 5071.
11 B. Adams, C. Radtke, R. Black, M. Trudeau, K. Zaghib and L. Nazar, *Energy Environ. Sci.*, 2013, **6**, 1772; Y. Mo, S. Ong and G. Ceder, *Phys. Rev. B: Condens. Matter Mater. Phys.*, 2011, **84**, 205446; Y. Li, J. Wang, X. Li, D. Geng, M. N. Banis, Y. Tang, D. Wang, R. Li, T.-K. Sham and X. Sun, *J. Mater. Chem.*, 2012, **22**, 20170.
12 C. Laoire, S. Mukerjee and K. Abraham, *J. Phys. Chem. C*, 2009, **113**, 20127.
13 P. Hartmann, C. Bender, J. Sann, A. Dürr, M. Jansen, J. Janek and P. Adelhelm, *Phys. Chem. Chem. Phys.*, 2013, **15**, 11661.